The Balance of Salinity Variance in a Partially Stratified Estuary: Implications for Exchange Flow, Mixing, and Stratification

TAO WANG

*College of Oceanography, Hohai University, Nanjing, and State Key Laboratory of Marine
Environmental Science, Xiamen University, Xiamen, China*

W. ROCKWELL GEYER

Woods Hole Oceanographic Institution, Woods Hole, Massachusetts

ABSTRACT

Salinity variance dissipation is related to exchange flow through the salinity variance balance equation, and meanwhile its magnitude is also proportional to the turbulence production and stratification inside the estuary. As river flow increases, estuarine volume-integrated salinity variance dissipation increases owing to more variance input from the open boundaries driven by exchange flow and river flow. This corresponds to the increased efficient conversion of turbulence production to salinity variance dissipation due to the intensified stratification with higher river flow. Through the spring–neap cycle, the temporal variation of salinity variance dissipation is more dependent on stratification than turbulence production, so it reaches its maximum during the transition from neap to spring tides. During most of the transition time from spring to neap tides, the advective input of salinity variance from the open boundaries is larger than dissipation, resulting in the net increase of variance, which is mainly expressed as vertical variance, that is, stratification. The intensified stratification in turn increases salinity variance dissipation. During neap tides, a large amount of enhanced salinity variance dissipation is induced by the internal shear stress near the halocline. During most of the transition time from neap to spring tides, dissipation becomes larger than the advective input, so salinity variance decreases and the stratification is destroyed.

1. Introduction

In estuaries, the exchange between ocean and river water is fundamentally important to the dynamics (Hansen and Rattray 1965) as well as biogeochemical processes such as nutrient fluxes, hypoxia, and contaminant transport (Sutherland et al. 2011). Exchange flow is not simply an advective process, because in order for exchange to occur, the incoming saltwater must be mixed with freshwater, as described by the Knudsen relation for estuarine exchange flow (Knudsen 1900).

Therefore, the mixing of salinity is an essential ingredient of exchange flow.

Before examining in detail the relationship between exchange flow and mixing of salinity, it is important to establish a clear, quantitative definition of "mixing of salinity." In the ocean turbulence community, the mixing of a tracer is defined by the tracer variance dissipation rate (Osborn and Cox 1972; Stern 1968; Nash and Moum 1999). This quantity was used by Burchard et al. (2009) to quantify the mixing of salinity in the Baltic Sea, and Becherer and Umlauf (2011) developed a temperature variance framework to study the mixing of temperature in lakes. Two recent studies have examined the relationship between exchange flow and the mixing of salinity in estuaries (Wang et al. 2017; MacCready et al. 2018). Wang et al. (2017) first quantified the estuarine volume-integrated salinity variance dissipation in an estuary based on the

---

Corresponding author: Tao Wang, haidawangtao@163.com; taowang@hhu.edu.cn

exchange flow, using the Hudson River estuary as a case study, based on the total exchange flow (TEF) transformation of the salt flux into salinity coordinates. While they established the relationship between exchange flow and salinity mixing, they did not frame the relationship in terms of the salinity variance equation. MacCready et al. (2018) also addressed the relationship between exchange flow and salinity variance dissipation, but using the conservation of salinity variance as a framework for the analysis. Using Knudsen relations (Knudsen 1900) to address the time-average regime, they derived a remarkably simple expression linking the exchange flow to the volume-integrated mixing of salinity and demonstrated its utility in a numerical simulation of an idealized estuary with constant river flow and a spring–neap modulation of tidal amplitude.

While the equations in MacCready et al. (2018) provide an integrated measure of the balance of salinity variance in an estuary, they do not address the mechanisms for the variations with river flow and spring–neap cycle and the mixing processes inside the estuary that actually accomplish this balance.

Total salinity variance can be decomposed into vertical and horizontal salinity variance, and vertical salinity variance can be used to represent the strength of stratification (Li et al. 2018). Stratification influences the strength of salinity variance dissipation, because it links salinity variance dissipation and turbulent buoyancy flux to turbulence production. Therefore, stratification (or vertical variance) links turbulence production to salinity variance dissipation, then to exchange flow through the salinity variance balance equations, and the relationships among them may shed light on the mechanisms of their variability with river flow and the spring–neap cycle.

In the present paper, to understand the mechanisms of their variability with river flow and tidal amplitudes in a realistic estuarine domain, we use the numerical model of the Hudson estuary to study the mixing processes inside the estuary, including salinity variance dissipation, turbulent buoyancy flux, and turbulence production, and how these mixing processes relate to exchange flow under different river conditions and spring–neap cycle in a partially stratified estuary.

The paper is organized as follows. In section 2, we briefly describe the numerical model of the Hudson estuary, the salinity variance balance equations, and the theoretical relationship among salinity variance dissipation, turbulent buoyancy flux, and turbulence production. In section 3, we examine the salinity variance balance in the Hudson estuary under steady state and study the variations of exchange flow, salinity variance dissipation, turbulent buoyancy flux, and turbulence production with river flow. In section 4, the influence of the spring–neap cycle on the variations of exchange flow, salinity variance dissipation, turbulent buoyancy flux, and turbulence production and the related mechanisms are studied. Section 5 presents the discussion and conclusions.

2. Methods

a. Numerical model of the Hudson estuary

The Hudson estuary model setup is identical to that used by Wang et al. (2017), which is based on a series of validated ROMS model studies (Warner et al. 2005a; Warner et al. 2010). The model consists of a 1133 × 530 × 16 curvilinear grid, including the New York Harbor, the Hudson estuary, and the East River. In the present paper, the estuarine region for analyzing is chosen from the Battery, that is, the mouth of the Hudson estuary, to the end of salt intrusion. Parameterizations for vertical eddy viscosity and diffusivity are determined using the k–ε turbulence closure scheme with the Canuto-A stability functions (Umlauf and Burchard 2005; Warner et al. 2005b). The horizontal diffusivity is set to be 0, so the horizontal mixing of salinity is neglected in the following analysis of this paper. To get the main features of tides in the Hudson estuary and study the balance between exchange flow and salinity variance dissipation for stationary forcing conditions, the ocean boundary is forced by M_2 and S_2 tidal constituents to simulate spring–neap variations. The river discharge in the Hudson estuary typically varies about from 150 to $2000\,\mathrm{m^3\,s^{-1}}$ between low and high discharge conditions. To study the response of the estuary to river flow under steady state, four cases are simulated with different constant river discharges at the river boundary, which are 200, 500, 1000, and $2000\,\mathrm{m^3\,s^{-1}}$ (Fig. 1).

b. The balance equations of estuarine salinity variance

Following MacCready et al. (2018), the estuarine volume-integrated salinity variance, that is, total salinity variance, is defined as

$$\mathrm{SVAR} = \iiint_V s'^2 \, dV, \qquad (1)$$

where V indicates the whole estuarine volume, that is, from the estuarine mouth to the river end where no salt reaches, and $s'^2 = (s - \bar{s})^2$, where $\bar{s}$ indicates the estuarine volume-averaged salinity. The tidally
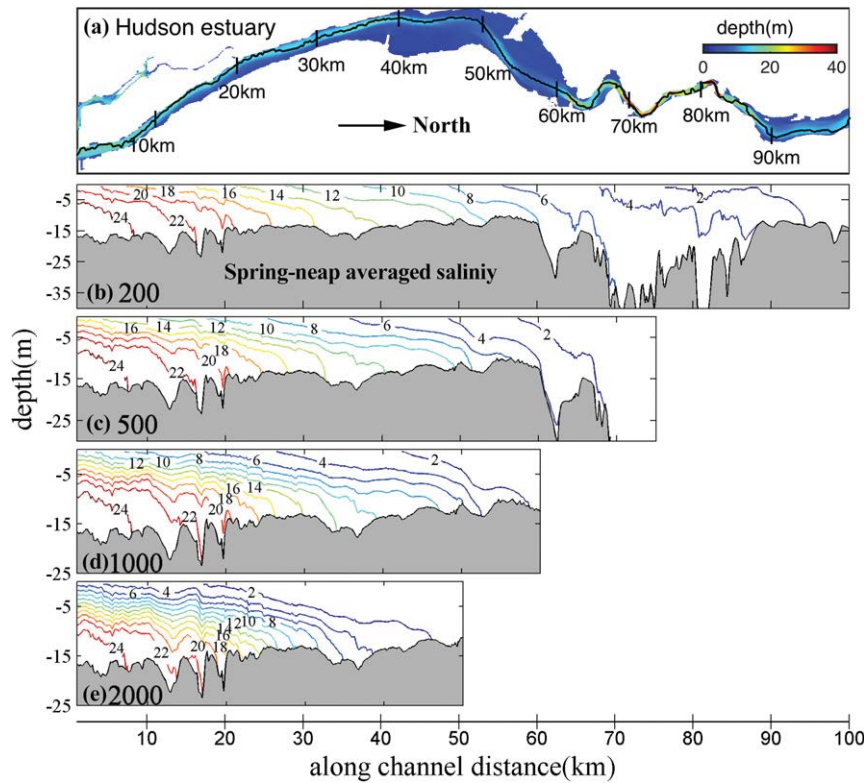
FIG. 1. (a) The Hudson estuary bathymetry, with the black line denoting the thalweg. The rightward direction in the figure indicates the north direction. (b)–(e) Model-generated spring–neap-averaged thalweg salinity with river discharge of 200, 500, 1000, and 2000 $\mathrm{m^3\,s^{-1}}$, respectively.

averaged conservation of the estuarine salinity variance is written as

$$\underbrace{\left\langle \frac{\partial}{\partial t} \iiint_V s'^2\, dV \right\rangle}_{\text{Temporal variation}} = \underbrace{(Q_{\text{in}} S_{\text{in}}'^2 + Q_{\text{out}} S_{\text{out}}'^2 + Q_R \overline{S}^2)}_{\text{Advection}}$$

$$- \underbrace{\left\langle \iiint_V \chi_s\, dV \right\rangle}_{\text{Salinity variance dissipation}} , \qquad (2)$$

where $\langle \ \rangle$ indicates the tidal average; χ_s indicates the salinity variance dissipation; and Q_R, Q_{in}, Q_{out}, $S_{\text{in}}'^2$, and $S_{\text{out}}'^2$ indicate the tidally averaged river discharge, inflow and outflow volume flux, and flux-weighted s'^2 at the mouth quantified with TEF analysis, respectively. The symbol $\overline{S}^2$ indicates the tidally averaged salinity variance transported by river flow, which satisfies $\overline{S}^2 = \langle \overline{s}^2 \rangle$. Note that Q_{out} is defined to be negative, and salinity variance dissipation is defined to be positive. The detailed mathematical quantification of Q_{in}, Q_{out}, and the flux-weighted salinities and s'^2 with TEF analysis can refer to MacCready (2011). Under steady state, for example,

when all the terms in Eq. (2) are averaged with one spring–neap cycle and with the approximation of $S_{\text{in}}'^2 \approx (S_{\text{in}} - \langle \overline{s} \rangle)^2$ and $S_{\text{out}}'^2 \approx (S_{\text{out}} - \langle \overline{s} \rangle)^2$, a simple expression linking the exchange flow to the volume-integrated salinity variance dissipation under steady state can be derived:

$$\left\langle \iiint_V \chi_s\, dV \right\rangle_{\text{SN}} \approx Q_R S_{\text{in}} S_{\text{out}} = Q_{\text{in}} S_{\text{in}} (S_{\text{in}} - S_{\text{out}}), \quad (3)$$

where $\langle \ \rangle_{\text{SN}}$ indicates the time averaging for steady state, which is usually chosen as spring–neap cycle averaging, and S_{in} and S_{out} indicate the inflow and outflow flux-weighted salinities quantified with TEF analysis, respectively. The "$\approx$" expression is used because the nonuniformity of inflow and outflow salinities induces small errors in the equation. The application of Eq. (3) in the Hudson estuary is examined in section 3.

Equations (2) and (3) reveal the balance between exchange flow and salinity variance dissipation integrated over the estuarine volume. To study how salinity variance is dissipated inside the estuary, we consider the

relationship among salinity variance dissipation, turbulent buoyancy flux, turbulence production, and stratification, as discussed next.

c. Relationship among salinity variance dissipation, turbulent buoyancy flux, and turbulence production

Turbulence production and background stratification are the necessary elements for salinity variance dissipation. Turbulent buoyancy flux is an important quantity to link salinity variance dissipation to turbulence production. Because horizontal mixing is neglected in the model, according to Osborn and Cox (1972), with the assumption of a stationary, high Reynolds number turbulence condition and small influence of molecular diffusivity on turbulent production, the relationship between salinity variance dissipation and turbulent buoyancy flux can be written as

$$\chi_s \approx 2K_z \left(\frac{\partial s}{\partial z}\right)^2 = \frac{2B}{\beta g}\frac{\partial s}{\partial z},$$ (4)

where K_z indicates the vertical diffusivity quantified with the turbulence closure scheme, β is the coefficient of saline contraction $[\beta = 7.7 \times 10^{-4}~(\mathrm{g\,kg^{-1}})^{-1}]$, g is the gravitational acceleration, z indicates the vertical coordinate with upward direction, and B indicates turbulent buoyancy flux, which can be written as

$$B = g\beta K_z \partial s/\partial z.$$ (5)

Therefore, salinity variance dissipation and turbulent buoyancy flux both depend on the strength of stratification. Turbulent buoyancy flux can be related to the magnitude of turbulence production via the flux Richardson number (Osborn 1980; Moum 1996):

$$B = -R_f P,$$ (6)

where P is the turbulence production and R_f is the flux Richardson number (Holleman et al. 2016; Gregg et al. 2018). The flux Richardson number provides a straightforward linkage between turbulent buoyancy flux and turbulence production, so we use it to study the relationship between turbulent buoyancy flux and turbulence production in the present paper. Winters et al. (1995) provides a robust definition of "mixing efficiency" that is defined as the ratio of background potential energy to turbulent kinetic energy dissipation, which puts particular emphasis on the irreversible transfer from turbulence production to potential energy. In the present paper, the conversion rate of turbulence production to turbulent buoyancy flux in the whole estuary is defined as

$$\hat{R}_f = -\iiint_V \rho B\, dV \Big/ \iiint_V \rho P\, dV.$$ (7)

In an estuary, the vertical shear production is the dominant source of turbulence production, which can be expressed using turbulence closure as

$$P = K_m \left[\left(\frac{\partial u}{\partial z}\right)^2 + \left(\frac{\partial v}{\partial z}\right)^2\right],$$ (8)

where K_m indicates the vertical eddy viscosity quantified with the turbulent closure scheme. When calculating the estuarine integral of shear production with the numerical model results, the significant fraction coming from the lower half of the lowermost grid cell is also considered, which is calculated with the lower-half grid volume integral of $(1/\rho)[|\tau_b^x(u_b/z_b)| + |\tau_b^y(v_b/z_b)|]$, where τ_b^x and τ_b^y indicate the bottom shear stress, u_b and v_b indicate the velocities in the lowest grid cell, and z_b is the distance of the lowest grid cell center to the bottom.

Through combining Eq. (4) with Eq. (6), the relationship between salinity variance dissipation and shear production can be obtained:

$$\chi_s = \frac{2}{\beta g}\frac{\partial s}{\partial z}B = -\left(\frac{2R_f}{\beta g}\frac{\partial s}{\partial z}\right)P.$$ (9)

As shown in Eqs. (5) and (9), the strength of stratification has a great influence on the magnitudes of turbulent buoyancy flux and salinity variance dissipation. The strength of stratification can also be related to total salinity variance inside the estuary, that is, the left term in Eq. (2).

d. Decomposition of salinity variance

Total salinity variance inside the estuary can be decomposed into vertical and horizontal salinity variance (Li et al. 2018):

$$\iiint_V s'^2\, dV = \iiint_V s_v'^2\, dV + \iiint_V s_h'^2\, dV,$$ (10)

where $\iiint_V s_v'^2\, dV$ and $\iiint_V s_h'^2\, dV$ indicate the estuarine volume-integrated vertical and horizontal salinity variance, respectively, and $s_v'^2$ is defined by $s_v'^2 = (s - \bar{s}_v)^2$, where the symbol "$\bar{}_v$" indicates the vertical average at each profile. The vertical salinity variance is directly related to the strength of stratification. In this paper, we use the volume-averaged vertical salinity variance, that is, $\iiint_V s_v'^2\, dV/V$, to represent the strength of stratification to make it more convenient to compare to the stratification in other estuaries in future studies. The horizontal variance is obtained by subtracting the vertical variance from the total variance. It is usually the dominant

component of total variance (Li et al. 2018), and it provides the salinity variations that produce baroclinic pressure gradients in estuaries.

3. Variations of exchange flow and mixing processes with river flow

In this section, the Hudson estuary model outputs are used to test the validity of Eq. (3) in representing the relationship between salinity variance dissipation and exchange flow in a realistic domain. We also study the influence of the variations of river flow on exchange flow and mixing processes.

By averaging over a spring–neap cycle, the time-averaged regime under different river flow conditions is assessed. As river discharge increases, the salt intrusion becomes shorter and stratification becomes stronger (Fig. 1), as expected from classical estuarine theory (MacCready and Geyer 2010). The TEF calculations of exchange flow and flux-weighted salinities (averaged over the spring-neap cycle) for the different river discharge cases are shown in Figs. 2a and 2b. While the outflow volume Q_{out} and outflow salinity S_{out} vary strongly with river flow Q_R, the inflow volume flux Q_{in} and inflow salinity S_{in} are almost invariant with river flow. A similar result is also found by MacCready (2011) in application to the Columbia River estuary. The relationships among these variables are consistent with the Knudsen relations.

Using TEF analysis, the advective salinity variance fluxes at the open boundaries are quantified (Fig. 2c). When calculating the estuarine volume-averaged variables, the estuarine volume is chosen from the estuarine mouth to the river end where no salt reaches. Therefore, for different river flow conditions, because the length of salt intrusion differs, the estuarine volume for calculating is different. As river discharge Q_R increases, the incoming salinity variance flux $Q_{in}S_{in}'^2$ driven by the inflow of exchange flow is almost invariant, but the salinity variance input due to river discharge $Q_R\overline{S}^2$ increases, and the outgoing salinity variance flux $-Q_{out}S_{out}'^2$ driven by the outflow of exchange flow decreases, resulting in a net input of salinity variance that increases with river flow.

As Eq. (2) shows, the net input of salinity variance balances the estuarine volume-integrated salinity variance dissipation under steady-state conditions. Here we define the volume-integrated salinity variance dissipation quantified with the convergence of the advective terms in Eq. (2) as the full salinity variance dissipation (green asterisks in Fig. 3). Because horizontal and molecular mixing are neglected in the model, the spring–neap averaged and estuarine volume-integrated model-resolved
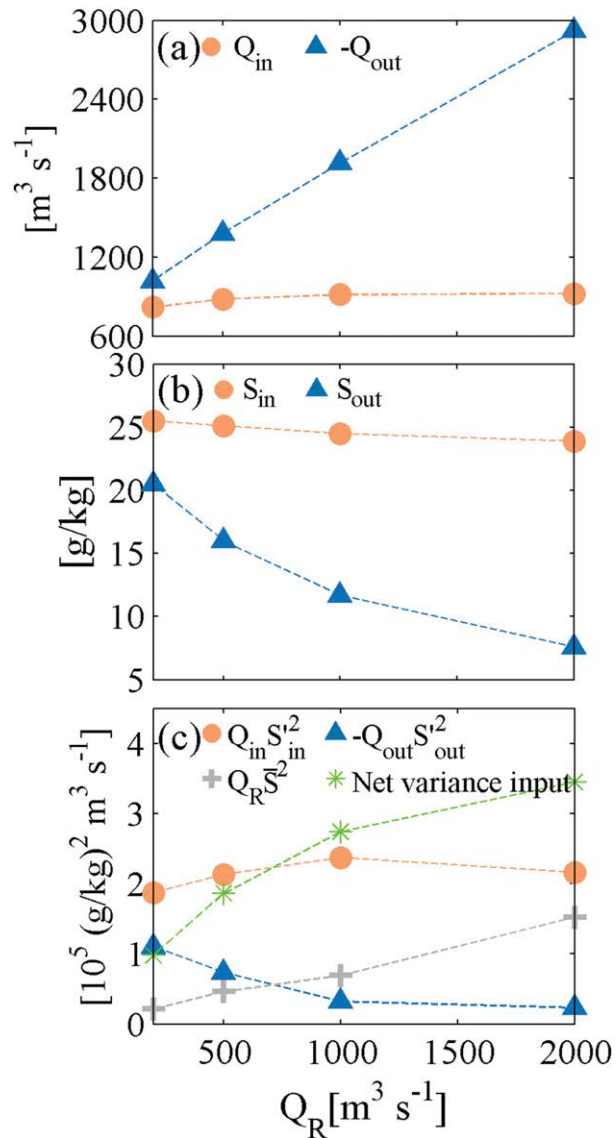

FIG. 2. Dependence of exchange flow and advective variance fluxes on river discharge, including (a) spring–neap-averaged inflow volume flux Q_{in} (orange dots) and outflow volume flux $-Q_{out}$ (blue triangles) at the mouth for four different river discharges. (b) Spring–neap-averaged flux-weighted inflow salinity S_{in} and outflow salinity S_{out} at the mouth. (c) Magnitudes of the terms in Eq. (2), including advective salinity variance flux driven by exchange flow at the mouth (orange dots and blue triangles) and by river flow (gray plus signs), and net salinity variance input (green asterisks), which is equal to the dissipation term in Eq. (2).

dissipation due to vertical mixing can be quantified with $\left\langle \iiint_V 2K_z(\partial s/\partial z)^2 \, dV \right\rangle_{SN}$ (gray triangles in Fig. 3). The near-agreement between the full dissipation and model-resolved dissipation indicates that the net input of salinity variance is approximately balanced by the model-resolved salinity variance dissipation due to vertical mixing.
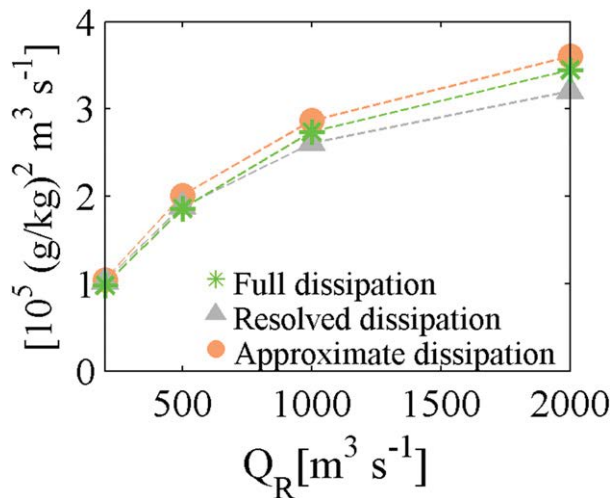
FIG. 3. Comparison of the full, model-resolved and approximate estuarine volume-integrated salinity variance dissipation. The green asterisks indicate the full salinity variance dissipation quantified with the convergence of the advective terms in Eq. (2), which are the same as the green asterisks in Fig. 2. It includes both the model-resolved dissipation due to physical mixing and unresolved dissipation due to numerical mixing. The gray triangles indicate the model-resolved salinity variance dissipation due to physical mixing, which are quantified with the model-resolved diffusivity K_z. The orange dots indicate the approximate salinity variance dissipation quantified with Eq. (3).

The small difference is caused by numerical mixing, which provides an additional sink of salinity variance. Equation (2) can therefore be used to estimate the estuarine integral of salinity variance dissipation due to numerical mixing (Burchard and Rennau 2008). The magnitude of salinity variance dissipation due to numerical mixing is less than 5% of the full salinity variance dissipation in the Hudson estuary model.

The integrated salinity variance dissipation can also be approximated using the simple relation in Eq. (3) with the values of Q_{in}, S_{in}, and Q_R. This approximation (orange dots in Fig. 3) slightly overestimates the exactly full salinity variance dissipation (green asterisks in Fig. 3), revealing that under steady-state conditions, exchange flow and salinity variance dissipation in the Hudson estuary roughly satisfy the simple relationship as Eq. (3) shows. The errors mainly come from the approximations of $S_{out}'^2 \approx (S_{out} - \langle \bar{s} \rangle)^2$ and $S_{in}'^2 \approx (S_{in} - \langle \bar{s} \rangle)^2$. If the inflow and outflow salinities were uniform, Eq. (3) would be exact.

Next we consider the influence of river flow on the mixing mechanisms. As shown in Eq. (9), the magnitude of salinity variance dissipation depends on the magnitudes of shear production and stratification inside the estuary. Using Eqs. (5) and (8), the estuarine volume-integrated and spring–neap-averaged shear production $\langle \iiint_V \rho P \, dV \rangle_{SN}$ and turbulent buoyancy flux $-\langle \iiint_V \rho B \, dV \rangle_{SN}$ for the four different river discharges are quantified, with the results shown in Table 1. Also shown are volume averages of these quantities. Estuarine volume-averaged vertical salinity variance is quantified to represent the strength of stratification. As river discharge increases, the estuary becomes shorter, resulting in a decrease in the estuarine integral of shear production. Note that the volume-averaged shear production actually increases slightly with river discharge, due to the increased shear associated with the increasing river flow. Estuarine volume-integrated turbulent buoyancy flux is almost invariant, due to the enhanced stratification (vertical salinity variance) with higher river flow, thus increasing the ratio of turbulent buoyancy flux to shear production, that is, $\langle \hat{R}_f \rangle_{SN}$ is increased. Salinity variance dissipation increases with river flow, as already described in context with the increasing input of salinity variance. The increase in turbulent buoyancy flux and salinity variance dissipation with discharge are both due to the increased stratification, that is, vertical salinity variance, which increases by more than a factor of 10 between low and high discharge (Table 1).

The relationship between turbulent buoyancy flux and shear production is quantified by the flux Richardson number. An analogous parameter can be defined that quantifies how effectively shear production contributes to the salinity variance dissipation in an estuary. We define a nondimensional parameter that we will call the "mixing ratio" ξ as

$$\xi = \rho_0 \beta g \frac{h_0}{s_0} \frac{\iiint_V \chi_s \, dV}{\iiint_V \rho P \, dV}, \tag{11}$$

where h_0 and s_0 indicate the estuarine mean depth and maximum salinity at the estuarine mouth, respectively. As shown in Table 1, the spring–neap-averaged parameter $\langle \xi \rangle_{SN}$ increases with river discharge, indicating a larger proportion of shear production contributes to salinity variance dissipation. It has the same tendency as R_f, but its amplitude shows more variation, because salinity variance dissipation is even more sensitive to stratification than turbulent buoyancy flux. Estuaries with low values of ξ do little mixing of salinity relative to turbulence production, whereas high values of ξ indicate "efficient" mixing of salinity. As the analysis in the following section will demonstrate, the value of ξ varies markedly through the spring–neap cycle, again because of the sensitive dependence of ξ on stratification.

TABLE 1. Spring–neap-averaged magnitudes of shear production, turbulent buoyancy flux, and salinity variance dissipation under different river discharge conditions. Both of the estuarine volume-integrated and volume-averaged values are shown. The estuarine volume-averaged vertical salinity variance $\langle \iiint_V s_v'^2\, dV/V \rangle_{\mathrm{SN}}$ is used to represent the strength of stratification. The nondimensional ratios $\hat{R}_f$ and ξ are obtained using Eqs. (7) and (10). The symbol $\langle\ \rangle_{\mathrm{SN}}$ in this table indicates spring–neap averaging. When calculating ξ, we use $h_0 = 10\,\mathrm{m}$ and $s_0 = 25\,\mathrm{g\,kg^{-1}}$ for the Hudson estuary.

$Q_R\ (\mathrm{m^3\,s^{-1}})$	200	500	1000	2000
$\langle \iiint_V \rho P\, dV \rangle_{\mathrm{SN}}$ (MW)	21	19	16	11
$\langle \iiint_V \rho P\, dV/V \rangle_{\mathrm{SN}}\ (10^{-2}\,\mathrm{W\,m^{-3}})$	1.3	1.4	1.5	1.6
$-\langle \iiint_V \rho B\, dV \rangle_{\mathrm{SN}}$ (MW)	1.0	0.99	0.96	0.81
$-\langle \iiint_V \rho B\, dV/V \rangle_{\mathrm{SN}}\,(10^{-3}\,\mathrm{W\,m^{-3}})$	0.64	0.75	0.95	1.2
$\langle \iiint_V \chi_s\, dV \rangle_{\mathrm{SN}}$ $[10^5\,(\mathrm{g\,kg^{-1}})^2\,\mathrm{m^3\,s^{-1}}]$	0.98	1.9	2.7	3.5
$\langle \iiint_V \chi_s\, dV/V \rangle_{\mathrm{SN}}$ $[10^{-4}\,(\mathrm{g\,kg^{-1}})^2\,\mathrm{s^{-1}}]$	0.64	1.4	2.7	5.2
$\langle \iiint_V s_v'^2\, dV/V \rangle_{\mathrm{SN}}\ [(\mathrm{g\,kg^{-1}})^2]$	0.21	0.74	1.3	2.5
$\langle \hat{R}_f \rangle_{\mathrm{SN}}$	0.049	0.052	0.062	0.075
$\langle \xi \rangle_{\mathrm{SN}}$	0.014	0.030	0.053	0.096

4. Variations of exchange flow and mixing with spring-neap tides

a. Balance of salinity variance during the spring–neap cycle

Whereas the spring–neap-averaged result represents a simple balance between advective inputs and dissipation of salinity variance, the intensity of the various terms varies considerably through the spring-neap cycle due to the temporal variations of total salinity variance [the left-hand-side term in Eq. (2)]. In this section, the model results with intermediate river discharge conditions $500\,\mathrm{m^3\,s^{-1}}$ are used as an example to analyze the spring–neap variations. The spring–neap variations under the other river discharge conditions are similar to the results with river discharge of $500\,\mathrm{m^3\,s^{-1}}$. The tidally averaged

values in the following analysis are all obtained through 33-h low-pass filtering.

Using Eq. (10), the spring–neap variations of tidally averaged total, vertical, and horizontal salinity variance are quantified (Fig. 4). Total variance peaks just after neap tides, with a minimum just after spring tides. Horizontal variance shows a similar but much more subtle spring–neap variation, but vertical variance shows marked spring–neap variation, almost vanishing during spring tides and contributing most of the increase of total salinity variance during neap tides.

Total salinity variance is supplied by the advective terms at the mouth and river end and is dissipated by the salinity variance dissipation. Vertical variance (stratification) in turn influences the magnitude of salinity variance dissipation. To study how total salinity variance, exchange flow, and salinity variance dissipation are balanced during the spring–neap cycle, the spring–neap variabilities of the individual terms in the salinity variance equation [Eq. (2)] are analyzed. The tidally averaged terms in Eq. (2) are shown in Fig. 5. Not only does the dissipation term vary due to changes in stratification and turbulence intensity through the spring–neap cycle, but the advective input of variance also varies due to changes in the strength of the exchange flow and the salinities of the inflowing and outflowing water. The advective input of variance reaches its peak just after neap tides, and the dissipation term peaks between neap and spring. The competition between the advective input and dissipation results in the temporal variation of total salinity variance inside the estuary, which increases during the transition from spring to neap tides, and decreases during the transition from neap to spring tides.

The elements of the advective salinity variance input are shown in Fig. 6. River flow and the inflow branch of exchange flow always drive salinity variance into estuary, and the outflow branch of exchange flow removes
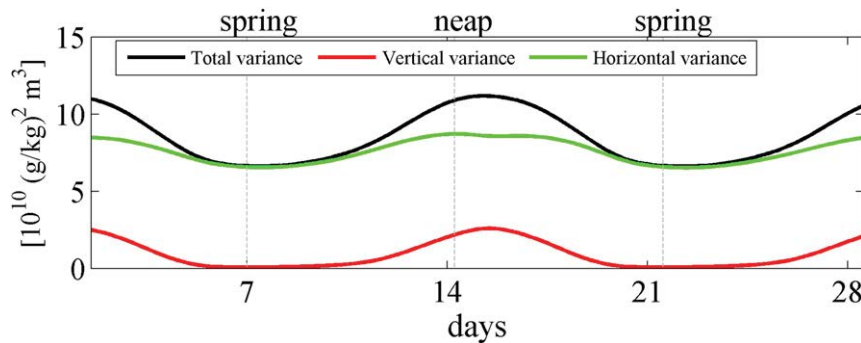

FIG. 4. Spring–neap variations of the estuarine volume-integrated and tidally averaged total, vertical, and horizontal salinity variance inside the estuary under a $500\,\mathrm{m^3\,s^{-1}}$ river discharge condition.
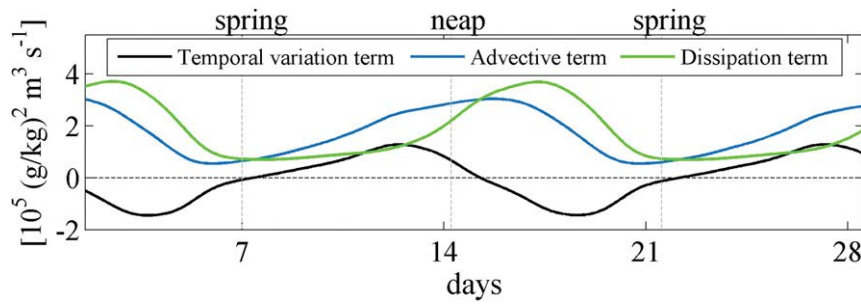
FIG. 5. Spring–neap variations of the three terms in Eq. (2) under a 500 m^3 s^{-1} river discharge condition.

salinity variance (Fig. 6a). Tidally averaged salinity variance flux driven by river flow is almost constant during the spring-neap cycle (Fig. 6a), so the variation of the net variance input mainly depends on the part that is driven by exchange flow, that is, $Q_{in}S'^2_{in} + Q_{out}S'^2_{out}$. As shown in Figs. 6b and 6c, during neap tides Q_{in} reaches its maximum, and S'^2_{out} is near to 0 because outflow salinity is near to $\langle \bar{s} \rangle$, so neap tides provide more net advective salinity variance flux into the estuary than spring tides (blue solid line in Fig. 6a). This increased net input of variance during neap tides is consistent with the observed strengthening of the exchange flow during the

neaps in the Hudson estuary by Bowen and Geyer (2003). It also explains in part the increase in salinity variance during the neaps (Fig. 5), but the spring–neap variations in salinity variance dissipation also must be considered, as discussed in the next section.

b. Mechanisms for the spring–neap variation of salinity variance dissipation

To study the mechanisms for the spring–neap variation of salinity variance dissipation, the relationship among the variations of salinity variance dissipation, turbulent buoyancy flux, shear production, and stratification
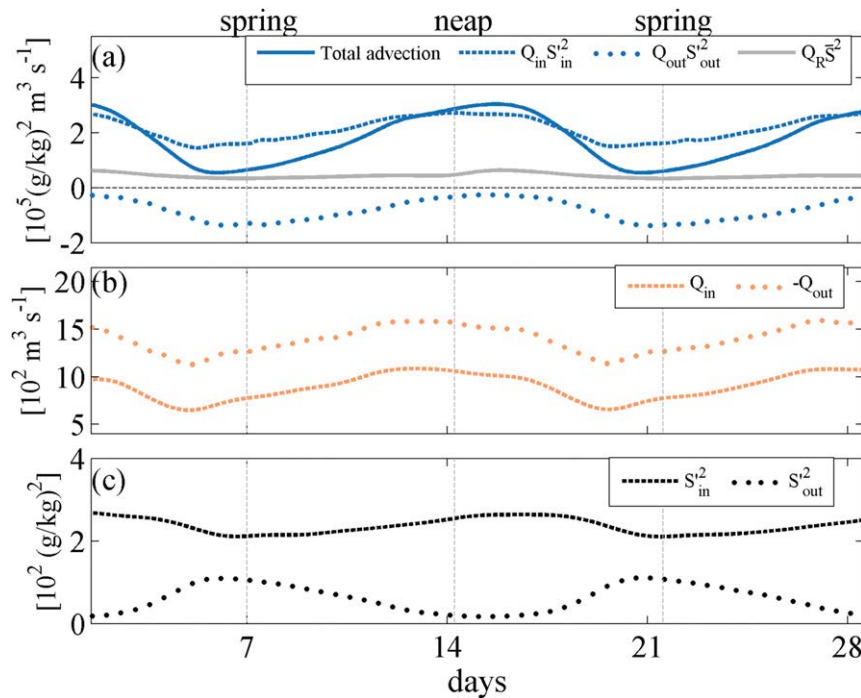

FIG. 6. Spring–neap variations of the elements of the advection term (blue line in Fig. 5) under a 500 m^3 s^{-1} river discharge condition, including (a) the salinity variance flux related to exchange flow and river flow. The blue solid line is the same as the blue line in Fig. 5. Note that Q_{out} is negative. (b) Inflow and outflow volume flux and (c) flux-weighted salinity variance.
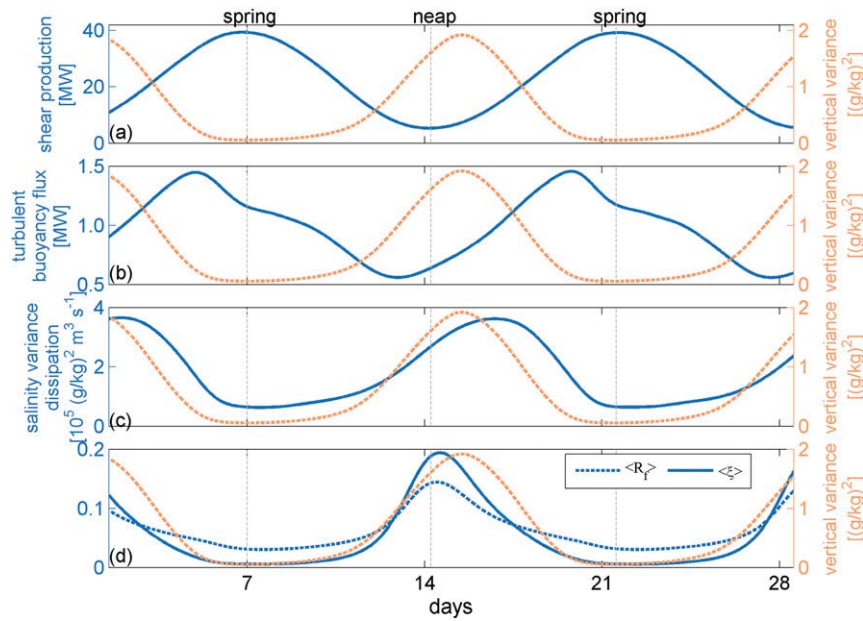
FIG. 7. Spring–neap variations of the tidally averaged and estuarine volume-integrated mixing variables under a $500\,\mathrm{m}^3\,\mathrm{s}^{-1}$ river discharge condition. The tidally and estuarine volume-averaged vertical salinity variance $\left\langle \iiint_V s_v'^2\,dV/V \right\rangle$, which indicates the strength of stratification inside the estuary, is overlaid on each panel, and its trend is similar to the red line in Fig. 4. The mixing variables shown in this figure include (a) shear production $\left\langle \iiint_V \rho P\,dV \right\rangle$; (b) turbulent buoyancy flux $-\left\langle \iiint_V \rho B\,dV \right\rangle$; (c) salinity variance dissipation $\left\langle \iiint_V \chi_s\,dV \right\rangle$, which is the same as the green line in Fig. 5; and (d) the ratio of turbulent buoyancy flux to turbulence production $\langle \hat{R}_f \rangle$ and the nondimensional ratio of salinity variance dissipation to turbulence production, i.e., mixing ratio $\langle \xi \rangle$.

is discussed. Figure 7 indicates that the maximum shear production occurs during maximum spring tide, but the maximum turbulent buoyancy flux occurs several days before maximum shear production (Fig. 7b). As Eq. (4) shows, compared to turbulent buoyancy flux, salinity variance dissipation is more sensitive to stratification, so the maximum salinity variance dissipation occurs closer to neap tides (Fig. 7c), when the stratification is maximal, as indicated by the vertical salinity variance (orange dashed lines on Fig. 7). Therefore, although shear production reaches its maximum due to strong tidal current amplitude, neither the turbulent buoyancy flux nor salinity variance dissipation reaches its maximum due to weak background stratification. In fact, the temporal variation of salinity variance dissipation is almost proportional to stratification (Fig. 7c) over the spring–neap cycle. Both the flux Richardson number and the mixing ratio $\langle \xi \rangle$ reach their maximum during neap tides (Fig. 7d), indicating larger proportion of turbulent production contributes to the turbulent buoyancy flux and salinity variance dissipation. Because salinity variance dissipation also quantitatively relates to exchange flow through Eq. (2), the mixing ratio $\langle \xi \rangle$ may provide the insights of how exchange flow varies with

shear production. During neap tides, the ratio is high owing to strong stratification, which corresponds to strong exchange flow (Fig. 6b); during spring tides, the ratio is near to zero because the estuary is nearly well mixed, and this corresponds to weak exchange flow.

The dependence of salinity variance dissipation on stratification is also clear in the spatial distributions of P, $-B$, and χ_s during maximum spring and minimum neap tides (Figs. 8, 9). During the spring tide, both the turbulent buoyancy flux and salinity variance dissipation mainly occur in the region influenced by the bottom boundary layer shear stress (Fig. 8). During the flood tide, turbulent buoyancy flux and salinity variance dissipation mainly occur above the bottom due to the weak stratification near the bottom (Fig. 8a). During the ebb tide, the structures of turbulent buoyancy flux and salinity variance dissipation are similar to shear production, which propagate from the bottom near to the surface (Fig. 8b). Shear production is also found to be enhanced at some sections with an abrupt change of depth along the channel, as discussed in detail in Wang et al. (2017). During the neap tide, bottom shear production is limited under the halocline (Fig. 9). Turbulent buoyancy flux occurs both in the bottom boundary layer and halocline,
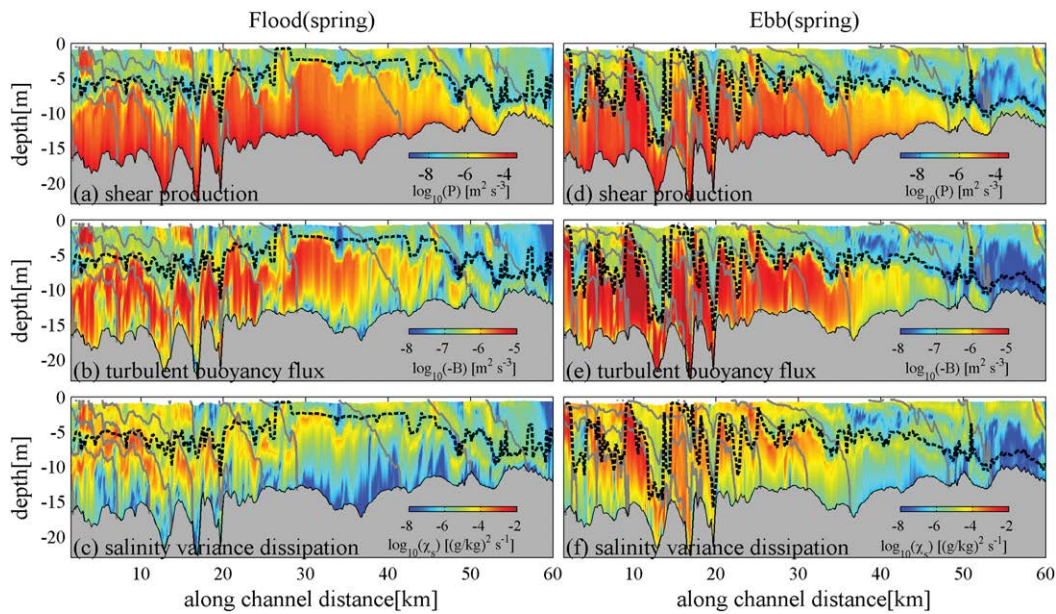
Fig. 8. Snapshots of the longitudinal distributions of shear production, turbulent buoyancy flux, and salinity variance dissipation at (a)–(c) flood and (d)–(f) ebb tides during the maximum spring tide. In (a) and (d), colors indicate the log values of shear production, and gray contours indicate the isohalines with a 2 g kg^{-1} interval. Colors indicate the log values of turbulent buoyancy flux in (b) and (c) and salinity variance dissipation in (e) and (f). The dashed black line in each panel indicates the line separating the bottom boundary layer and internal shear layer, which is used for the decomposition in Fig. 10.

especially during the flood tide. In contrast, most of the salinity variance dissipation occurs near the halocline, where stratification is the strongest (Fig. 9). Comparing spring to neap tides, even though the shear production is stronger during the spring tide than during the neap tide

(Figs. 8, 9), the magnitude of salinity variance dissipation is much smaller owing to weak stratification during spring tides (Fig. 8). The turbulent buoyancy flux is stronger during spring tides, because it is less sensitive to stratification than salinity variance dissipation.
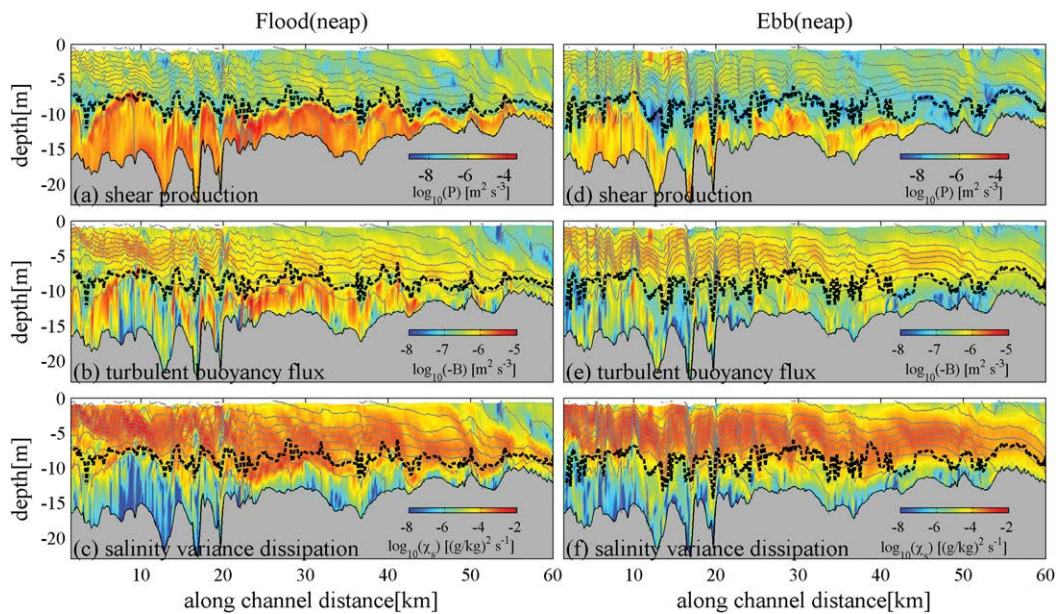

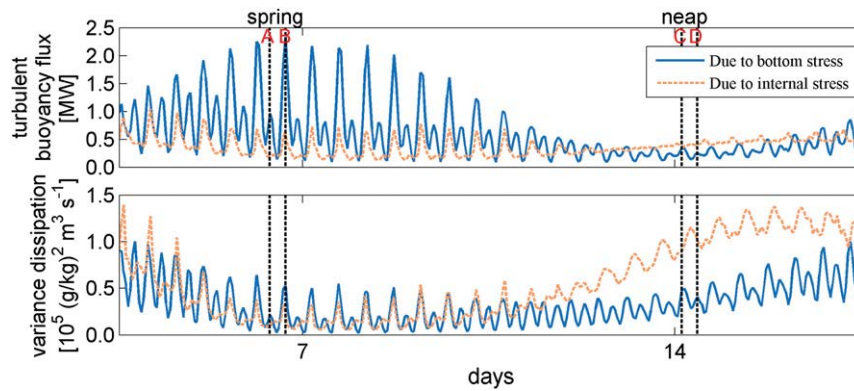Fig. 9. As in Fig. 8, but during the minimum neap tide.

FIG. 10. Spring–neap and tidal variations of (top) turbulent buoyancy flux and (bottom) salinity variance dissipation induced by bottom boundary layer shear stress and internal shear stress, respectively. The letters A, B, C, and D indicate the time of flood and ebb during maximum spring and minimum neap tides, respectively, i.e., corresponding to the time of the snapshots in Figs. 8 and 9.

The effects of wind and waves are not included in the Hudson estuary model, so the amount of turbulent buoyancy flux and salinity variance dissipation can be divided into two parts caused by two different mechanisms, respectively: the part that is generated at the bottom boundary layer and the other part that is caused by mixing within an internal shear layer. To quantitatively divide the salinity variance dissipation caused by the two mechanisms, we follow the method in Ralston et al. (2010), requiring a local minimum in shear stress to distinguish an internal shear layer from the bottom boundary layer. The turbulent buoyancy flux and salinity variance dissipation below the depth of stress minimum are attributed to bottom boundary layer shear and above the stress minimum are attributed to internal shear. As shown in Fig. 10, during spring tides, a larger part of the turbulent buoyancy flux is induced by the bottom boundary layer stress, and during neap tides, the turbulent buoyancy flux induced by the two mechanisms is comparable. In contrast, because of more sensitivity to stratification, salinity variance dissipation shows a much greater role in the internal shear stress during neap tides and has comparable contributions during spring tides.

5. Discussion and conclusions

We have studied the relationship among the variations of turbulence production, turbulent buoyancy flux, salinity variance dissipation, and stratification with river flow and the spring–neap cycle and how they are related to exchange flow in the Hudson estuary. As river flow increases, estuarine volume-integrated turbulence production decreases because salt intrusion becomes shorter, but salinity variance dissipation inside the estuary increases due to more net input of salinity variance, particularly from the increased river flow. The increased input of salinity variance during high river flow results in increased vertical variance, that is, increased stratification, which leads to more efficient conversion of turbulent energy to salinity variance dissipation, as quantified by the mixing ratio ξ. As a result, the dissipation of salinity variance keeps pace with the increased advective input during high flow conditions, even as volume-integrated turbulence production decreases because of the shortening of the salt intrusion.

Under unsteady-state conditions, as illustrated by the spring–neap cycle, the competition between the source, that is, advective input of variance driven by exchange flow and river flow, and the sink, that is, dissipation due to mixing, results in the temporal variation of total variance inside the estuary. Most of that variation in the Hudson is accounted for by the variation in vertical variance, with the horizontal variance remaining nearly constant. The vertical variance is uniquely associated with stratification, which strongly influences the magnitude of salinity variance dissipation, as quantified by the mixing ratio. The mixing ratio increases by more than an order of magnitude between spring and neap tides, leading to the dominance of salinity variance dissipation during neap tides. During neap tides, most of the salinity variance dissipation occurs in the halocline as a result of internal layer shear stress. During most of the transition time from spring to neap tides, the advective input of the variance is larger than the dissipation, resulting in the net increase of the total variance, as well as increasing the vertical and horizontal variance. Therefore, stratification is intensified, and salinity variance dissipation induced by internal shear stress increases near the halocline.

During most of the transition time from neap to spring tides, when dissipation becomes larger than the advective input of variance from the open boundaries, variance inside the estuary decreases and stratification is destroyed.

While this paper only considers the variance balance in the context with a single estuary, this approach has promise for comparing mixing processes between estuaries of different types. To remove the influence of different estuarine volumes, the volume-average estimates of shear production, turbulent buoyancy flux, and salinity variance dissipation shown in Table 1 would provide useful comparisons. For instance, MacDonald and Geyer (2004) reported turbulent buoyancy fluxes in the lift-off plume of the Fraser River of more than $10^{-4}\,\mathrm{m^2\,s^{-3}}$, more than two orders of magnitude higher than reported here. In the salt wedge of the Connecticut River, Holleman et al. (2016) reported local values of χ_s of more than 0.1 $(\mathrm{g\,kg^{-1}})^2\,\mathrm{s^{-1}}$, more than three orders of magnitude larger than the average values of the Hudson River. These are not fair comparisons, because neither the Fraser River nor Connecticut River values are estuarine averages, which would be expected to be considerably lower than the local values in regions of strong mixing. However it is likely that highly stratified estuaries will exhibit much higher values of χ_s and also of the mixing ratio ξ, given the sensitivity of these quantities to stratification. Likewise, well-mixed estuaries would be expected to have much lower values of these quantities than the Hudson estuary. Because of the central importance of mixing, stratification, and exchange flow to the estuarine regime, these comparisons of χ_s and ξ between estuaries should help better characterize the estuarine parameter space.

REFERENCES

Becherer, J. K., and L. Umlauf, 2011: Boundary mixing in lakes: 1. Modeling the effect of shear-induced convection. *J. Geophys. Res.*, **116**, C10017, https://doi.org/10.1029/2011JC007119.

Bowen, M. M., and W. R. Geyer, 2003: Salt transport and the time-dependent salt balance of a partially stratified estuary. *J. Geophys. Res.*, **108**, 3158, https://doi.org/10.1029/2001JC001231.

Burchard, H., and H. Rennau, 2008: Comparative quantification of physically and numerically induced mixing in ocean models. *Ocean Modell.*, **20**, 293–311, https://doi.org/10.1016/j.ocemod.2007.10.003.

——, F. Janssen, K. Bolding, L. Umlauf, and H. Rennau, 2009: Model simulations of dense bottom currents in the western Baltic Sea. *Cont. Shelf Res.*, **29**, 205–220, https://doi.org/10.1016/j.csr.2007.09.010.

Gregg, M. C., E. A. D'Asaro, J. J. Riley, and E. Kunze, 2018: Mixing efficiency in the ocean. *Annu. Rev. Mar. Sci.*, **10**, 443–473, https://doi.org/10.1146/annurev-marine-121916-063643.

Hansen, D. V., and M. Rattray, 1965: Gravitational circulation in straits and estuaries. *J. Mar. Res.*, **23**, 104–122.

Holleman, R. C., W. R. Geyer, and D. K. Ralston, 2016: Stratified turbulence and mixing efficiency in a salt wedge estuary. *J. Phys. Oceanogr.*, **46**, 1769–1783, https://doi.org/10.1175/JPO-D-15-0193.1.

Knudsen, M., 1900: Ein hydrographischer Lehrsatz (in German). *Ann. Hydrogr. Marit. Meteor.*, **28**, 316–320.

Li, X. Y., W. R. Geyer, J. R. Zhu, and H. Wu, 2018: The transformation of salinity variance: A new approach to quantifying the influence of straining and mixing on estuarine stratification. *J. Phys. Oceanogr.*, **48**, 607–623, https://doi.org/10.1175/JPO-D-17-0189.1.

MacCready, P., 2011: Calculating estuarine exchange flow using isohaline coordinates. *J. Phys. Oceanogr.*, **41**, 1116–1124, https://doi.org/10.1175/2011JPO4517.1.

——, and W. R. Geyer, 2010: Advances in estuarine physics. *Annu. Rev. Mar. Sci.*, **2**, 35–58, https://doi.org/10.1146/annurev-marine-120308-081015.

——, ——, and H. Burchard, 2018: Estuarine exchange flow is related to mixing through the salinity variance budget. *J. Phys. Oceanogr.*, **48**, 1375–1384, https://doi.org/10.1175/JPO-D-17-0266.1.

MacDonald, D. G., and W. R. Geyer, 2004: Turbulent energy production and entrainment at a highly stratified estuarine front. *J. Geophys. Res.*, **109**, C05004, https://doi.org/10.1029/2003JC002094.

Moum, J. N., 1996: Efficiency of mixing in the main thermocline. *J. Geophys. Res.*, **101**, 12 057–12 069, https://doi.org/10.1029/96JC00508.

Nash, J. D., and J. N. Moum, 1999: Estimating salinity variance dissipation rate from conductivity microstructure measurements. *J. Atmos. Oceanic Technol.*, **16**, 263–274, https://doi.org/10.1175/1520-0426(1999)016<0263:ESVDRF>2.0.CO;2.

Osborn, T. R., 1980: Estimates of local rate of vertical diffusion from dissipation measurements. *J. Phys. Oceanogr.*, **10**, 83–89, https://doi.org/10.1175/1520-0485(1980)010<0083:EOTLRO>2.0.CO;2.

——, and C. S. Cox, 1972: Oceanic fine structure. *Geophys. Fluid Dyn.*, **3**, 321–345, https://doi.org/10.1080/03091927208236085.

Ralston, D. K., W. R. Geyer, J. A. Lerczak, and M. Scully, 2010: Turbulent mixing in a strongly forced salt wedge estuary. *J. Geophys. Res.*, **115**, C12024, https://doi.org/10.1029/2009JC006061.

Stern, M. E., 1968: T–S gradients on the micro-scale. *Deep-Sea Res. Oceanogr. Abstr.*, **15**, 245–250, https://doi.org/10.1016/0011-7471(68)90001-6.

Sutherland, D. A., P. MacCready, N. S. Banas, and L. F. Smedstad, 2011: A model study of the Salish Sea estuarine circulation. *J. Phys. Oceanogr.*, **41**, 1125–1143, https://doi.org/10.1175/2011JPO4540.1.

Umlauf, L., and H. Burchard, 2005: Second-order turbulence closure models for geophysical boundary layers. A review

of recent work. *Cont. Shelf Res.*, **25**, 795–827, https://doi.org/10.1016/j.csr.2004.08.004.

Wang, T., W. R. Geyer, and P. MacCready, 2017: Total exchange flow, entrainment, and diffusive salt flux in estuaries. *J. Phys. Oceanogr.*, **47**, 1205–1220, https://doi.org/10.1175/JPO-D-16-0258.1.

Warner, J. C., W. R. Geyer, and J. Lerczak, 2005a: Numerical modeling of an estuary: A comprehensive skill assessment. *J. Geophys. Res.*, **110**, C05001, https://doi.org/10.1029/2004JC002691.

——, C. R. Sherwood, H. G. Arango, and R. P. Signell, 2005b: Performance of four turbulence closure models implemented using a generic length scale method. *Ocean Modell.*, **8**, 81–113, https://doi.org/10.1016/j.ocemod.2003.12.003.

——, W. R. Geyer, and H. G. Arango, 2010: Using a composite grid approach in a complex coastal domain to estimate estuarine residence time. *Comput. Geosci.*, **36**, 921–935, https://doi.org/10.1016/j.cageo.2009.11.008.

Winters, K. B., P. N. Lombard, J. J. Riley, and E. A. D'Asaro, 1995: Available potential energy and mixing in density-stratified fluids. *J. Fluid Mech.*, **289**, 115–128, https://doi.org/10.1017/S002211209500125X.